Available online at www.sciencedirect.com
SCIENCE DIRECT®
PERGAMON
Computers and Structures 81 (2003) 995–1008
Computers & Structures
www.elsevier.com/locate/compstruc

On optimal stabilized MITC4 plate bending elements for accurate frequency response analysis

Lonny L. Thompson

Department of Mechanical Engineering, Clemson University, Clemson, SC 29634-0921, USA

Abstract

The mixed interpolation technique of the well-established MITC4 quadrilateral plate finite element is combined with shear and generalized least-squares stabilization methods for accurate frequency response analysis. Dispersion analysis is used to determine optimal combinations of stabilization parameters, which, for a given mesh, provide for a three-fold increase in the frequency range over which accurate solutions are obtained, thus allowing for accurate solutions at significantly lower cost. Numerical results for the forced vibration of Reissner–Mindlin plates validate the observations made from the dispersion analysis.

Keywords: Stabilized finite element methods; Reissner–Mindlin plates; Plate finite elements; Dispersion analysis; Forced vibration; Frequency response analysis

1. Introduction

Accurate modeling of high-frequency response is important in many applications of structural dynamics, including modeling control–structure interactions, dynamic localizations, acoustic fluid–structure interaction, scattering from inhomogeneities, and other applications requiring precise modeling of dynamic characteristics. When modeling plate and shell structures, the inclusion of transverse shear deformation and rotary inertia effects such as that found in the well-known Reissner–Mindlin theory [1], is crucial for accurate response over a large frequency window.

Significant progress has been made on the mathematical stability and error analysis for Reissner–Mindlin plate finite elements for static analysis (see e.g. [2–7]). The simplist four-node quadrilateral elements use equal bilinear interpolation for both deflection and section rotations. Of these low order elements, the popular bilinear MITC4 element [8] based on mixed interpolation of shear strains has been established as a reliable and accurate element for static analysis. The error analysis [2,3] performed on this element showed that the MITC4 element is optimally convergent for deflections and rotations on regular meshes. However, as shown in [9], the MITC4 element may lose shear force accuracy for highly irregular meshes. Furthermore, for dynamic analysis, the MITC4 element exhibits significant wave number/frequency dispersion error. As a result, forced vibration response at intermediate to high frequencies will be misrepresented if a large number of elements are not used in the analysis; see [10]. From complex wave number dispersion analysis of the MITC4 element, it is found that over 20 elements per wavelength are required to obtain accurate solutions; a relatively high number compared to the rule-of-thumb of 10 elements per wavelength for bilinear quadrilateral elements for the scalar wave equation [12].

To address the shear force inaccuracy problem for static analysis, Lyly et al. [9], proposed a shear stabilization modification to the MITC4 element. This idea was introduced in early plate elements as a 'residual bending flexibility', designed to reduce shear stiffness, [13]. Later Stenberg and Lyly [14,15] showed that this

E-mail address: lonny.thompson@ces.clemson.edu (L.L. Thompson).

0045-7949/03/$ - see front matter
doi:10.1016/S0045-7949(02)00405-4

'trick' fits into a consistent variational method. The modification is simple to implement, in that it appears only as a redefinition of the shear modulus material parameter. Numerical studies performed in [9] showed that accuracy is improved with proper selection of the shear stabilization parameter. However, if the incorrect stabilization parameter is used, the deflection accuracy may decrease. To date, no criteria has been offered to select an optimal shear stabilization parameter, other than numerical experiment.

In this work, we combine the shear interpolation of the MITC4 plate element [8] with shear stabilization [9], with the residual-based, generalized least-squares methods developed in [10]. Using complex wave number dispersion analysis [16], optimal combinations of shear stabilization and generalized least squares stabilization parameters are determined which minimize wave number/frequency dispersion error. The reduction of dispersion error has a direct impact on the accuracy of frequency response for forced vibration problems. In particular, using dispersion accuracy as the design criteria, we define optimal combinations of stabilization parameters which, for a given mesh, provide for a threefold increase in the frequency range over which accurate solutions are obtained.

The paper is organized as follows: In Section 2 the Reissner–Mindlin plate bending problem for frequency response analysis is summarized. In Section 3 the new stabilized finite element method based on the MITC reduction technique combined with shear and generalized least-squares stabilization is presented. Section 4 gives the analytical wave number/frequency dispersion relation which is used to help design the optimal generalized least-squares stabilization parameters presented in Section 5. In Section 6 a complex wave number dispersion analysis is used to quantify the accuracy of different stabilization parameter combinations. In Section 7, a numerical example of forced vibration of a simply-supported plate is studied to verify the observations made from our dispersion analysis. Section 8 gives final conclusions.

2. Time-harmonic Reissner–Mindlin plate bending problem

We consider the Reissner–Mindlin plate bending model [1] with thickness t, two-dimensional midsurface $A \subset \mathbb{R}^2$, boundary ∂A, and transverse coordinate z. We consider a distributed load $f(x,y)$ and without loss of generality, assume a clamped plate. The plate displacement components, $(-z\beta_x, -z\beta_y, w)$, are parameterized by the vertical deflection of the midsurface $w(x,y)$, and independent angles $\boldsymbol{\beta} = (\beta_x, \beta_y)$, where $\beta_x(x,y)$, and $\beta_y(x,y)$ are defined by section rotations about the y and x axes, respectively. The material is assumed to be linear elastic, and isotropic. The motion is assumed time-harmonic and driven with circular frequency, ω.

The problem may be stated as: Given $f(x,y)$, E, ν, ρ, t, find $\boldsymbol{u} = (\boldsymbol{\beta}, \omega)$, over a given frequency band $\omega \in (\omega_1, \omega_2)$, such that,

$$R_1(\boldsymbol{u};\omega) := \operatorname{div}\boldsymbol{Q}(\boldsymbol{u}) + (\rho t\omega^2)w + f = 0, \quad (x,y) \in A \tag{1}$$

$$\boldsymbol{R}_2(\boldsymbol{u};\omega) := \operatorname{div}\boldsymbol{M}(\boldsymbol{\beta}) + \boldsymbol{Q}(\boldsymbol{u}) + (\rho I\omega^2)\boldsymbol{\beta} = \boldsymbol{0}, \quad (x,y) \in A \tag{2}$$

$$\boldsymbol{u} = 0, \quad (x,y) \in \partial A \tag{3}$$

where the moment tensor and shear vector are defined by,

$$\boldsymbol{M}(\boldsymbol{\beta}) := 2GI\left\{\boldsymbol{\epsilon}(\boldsymbol{\beta}) + \frac{\nu}{1-\nu}(\operatorname{div}\boldsymbol{\beta})\boldsymbol{I}\right\} \tag{4}$$

$$\boldsymbol{Q}(\boldsymbol{u}) := G\kappa t\boldsymbol{\gamma}(\boldsymbol{u}) = G\kappa t(\nabla w - \boldsymbol{\beta}) \tag{5}$$

with small curvature tensor,

$$\boldsymbol{\epsilon}(\boldsymbol{\beta}) := \tfrac{1}{2}(\nabla\boldsymbol{\beta} + (\nabla\boldsymbol{\beta})^{\mathrm{T}}) \tag{6}$$

Here, $I = t^3/12$, with Young's modulus E, Poisson's ratio ν, shear modulus $G = E/(2(1+\nu))$, and κ is a shear correction factor. In the above, $\nabla = (\partial_x, \partial_y)$ is the gradient vector, and 'div' stands for divergence, i.e., $\operatorname{div}\boldsymbol{\beta} = \partial_x\beta_x + \partial_y\beta_y$, and $\boldsymbol{I}$ is the unit tensor.

In the above, R_1 is a scalar residual associated with shear equilibrium, and $\boldsymbol{R}_2 = [R_{2x}, R_{2y}]^{\mathrm{T}}$ is a vector residual associated with moment equilibrium. Applying the divergence operator to the vector equation (2), and writing the bending and shear resultants in terms of $\boldsymbol{u} = (\boldsymbol{\beta}, w)$, the residuals can be restated in terms of the two scalar equations,

$$R_1(\boldsymbol{u};\omega) := (G\kappa t)\operatorname{div}\boldsymbol{\gamma} + (\rho t\omega^2)w + f = 0 \tag{7}$$

$$\begin{aligned} R_2(\boldsymbol{u};\omega) &:= \operatorname{div}\boldsymbol{R}_2 \\ &= (D_b\nabla^2 + \rho I\omega^2)\operatorname{div}\boldsymbol{\beta} + (G\kappa t)\operatorname{div}\boldsymbol{\gamma} = 0 \end{aligned} \tag{8}$$

where $D_b = EI/(1-\nu^2)$, $\nabla^2 = \operatorname{div}\nabla$, and $\boldsymbol{\gamma} = \nabla w - \boldsymbol{\beta}$.

The variational problem (weak form) may be stated as: Find the deflection and the rotation vector, $\boldsymbol{u} = (\boldsymbol{\beta}, w) \in [H_0^1(A)]^3$, such that,

$$\mathscr{B}(\boldsymbol{u},\boldsymbol{v};\omega) = (v,f), \quad \forall\boldsymbol{v} = (\boldsymbol{\alpha}, v) \in [H_0^1(A)]^3 \tag{9}$$

The symmetric, bilinear form is defined as,

$$\begin{aligned} \mathscr{B}(\boldsymbol{u},\boldsymbol{v}) :&= GIa(\boldsymbol{\alpha},\boldsymbol{\beta}) + G\kappa t(\nabla v - \boldsymbol{\alpha}, \nabla w - \boldsymbol{\beta}) \\ &\quad - \omega^2\{\rho t(v,w) + \rho I(\boldsymbol{\alpha},\boldsymbol{\beta})\} \end{aligned} \tag{10}$$

$$a(\boldsymbol{\alpha},\boldsymbol{\beta}) := 2\left\{(\boldsymbol{\varepsilon}(\boldsymbol{\alpha}), \boldsymbol{\varepsilon}(\boldsymbol{\beta})) + \frac{\nu}{1-\nu}(\operatorname{div}\boldsymbol{\alpha}, \operatorname{div}\boldsymbol{\beta})\right\} \tag{11}$$

The L_2-inner products are denoted by,

$$(v,w)_\Omega = \int_\Omega vw\,\mathrm{d}x\,\mathrm{d}y$$

$$(\boldsymbol{\alpha},\boldsymbol{\beta})_\Omega = \int_\Omega \boldsymbol{\alpha}\cdot\boldsymbol{\beta}\,\mathrm{d}x\,\mathrm{d}y$$

$$(\boldsymbol{\varepsilon}(\boldsymbol{\alpha}),\boldsymbol{\varepsilon}(\boldsymbol{\beta}))_\Omega = \int_\Omega \boldsymbol{\varepsilon}(\boldsymbol{\alpha}):\boldsymbol{\varepsilon}(\boldsymbol{\beta})\,\mathrm{d}x\,\mathrm{d}y$$

The subscript Ω is dropped when $\Omega = A$.

3. The stabilized MITC finite element methods

Consider a finite element mesh obtained by partitioning A into convex quadrilateral elements. Let A_e denote the area for a typical element number e. We then define $\mathscr{M}_h = \cup_e A_e$ as the union of element interiors. We consider equal order linear basis functions for the deflection and both components of the rotation. The finite element subspaces for the approximation of the deflection w^h and rotation vector $\boldsymbol{\beta}^h$ are,

$$W_h = \left\{w^h \in H_0^1(A), w^h|_{A_e} \in Q_1[A_e],\ \forall A_e \in \mathscr{M}_h\right\} \tag{12}$$

$$\boldsymbol{V}_h = \left\{\boldsymbol{\beta}^h \in H_0^1(A), \boldsymbol{\beta}^h|_{A_e} \in [Q_1(A_e)]^2,\ \forall A_e \in \mathscr{M}_h\right\} \tag{13}$$

where $Q_1(A_e)$ is the set of low-order polynomials of degree $\leqslant 1$ in each variable defined on the element area A_e.

The finite element interpolation of the element domain A_e, together with the displacement field w^h, and $\boldsymbol{\beta}^h$, follows the standard isoparametric procedure [18]. Define $\boldsymbol{\xi} = (\xi,\eta)$ to be natural coordinates on the reference bi-unit square $\hat{A}$ defined by the interval $[-1,1]^2$. The reference domain is then mapped onto the physical element domain A_e with cartesian coordinates $\boldsymbol{x} = (x,y)$ parameterized by,

$$\boldsymbol{x}(\xi,\eta) = \sum_{i=1}^{4} N_i(\xi,\eta)\boldsymbol{x}_i \tag{14}$$

where $\boldsymbol{x}_i = (x_i,y_i) \in \mathbb{R}^2$ are nodal coordinates, and N_i are bilinear shape functions,

$$N_i(\xi,\eta) = (1+\xi_i\xi)(1+\eta_i\eta)/4, \quad i = 1,\ldots,4 \tag{15}$$

$$N_{i,\xi} = \xi_i(1+\eta_i\eta)/4, \quad N_{i,\eta} = \eta_i(1+\xi_i\xi)/4$$

with nodal coordinates $(\xi_i,\eta_i) \in \{(-1,-1);(1,-1);(1,1);(-1,1)\}$. The displacements are constructed using the same bilinear functions:

$$w^h(\xi,\eta) = \sum_{i=1}^{4} N_i(\xi,\eta)w_i, \quad \boldsymbol{\beta}^h(\xi,\eta) = \sum_{i=1}^{4} N_i(\xi,\eta)\boldsymbol{\beta}_i \tag{16}$$

where w_i are nodal deflections and $\boldsymbol{\beta}_i = [\beta_x^i,\beta_y^i]$, are nodal rotations. Let $[\boldsymbol{J}]$ be the Jacobian transformation matrix of the mapping $\boldsymbol{x}:\hat{A}\to A_e$, i.e. $\widehat{\nabla} = [\boldsymbol{J}]^{\mathrm{T}}\nabla$, and $\nabla = [\boldsymbol{J}]^{-\mathrm{T}}\widehat{\nabla}$, where $\widehat{\nabla} = (\partial_\xi,\partial_\eta)$, and

$$[\boldsymbol{J}] := [\boldsymbol{x}_{,\xi}] = \begin{bmatrix} x_{,\xi} & x_{,\eta} \\ y_{,\xi} & y_{,\eta} \end{bmatrix} \tag{17}$$

3.1. MITC reduction technique

The assumed shear strain $\boldsymbol{\gamma}^h$ within an element, is interpolated with the MITC technique, [8], using a reduction operator $\boldsymbol{R}_h : [H^1(A_e)]^2 \to \boldsymbol{\Gamma}_h(A_e)$, which maps the shear strain interpolants evaluated from the spaces W^h and $\boldsymbol{V}^h$ to the assumed strain space $\boldsymbol{\Gamma}_h(A_e)$, [2–4]:

$$\boldsymbol{\Gamma}_h(A_e) = \left\{\boldsymbol{\gamma}|_{A_e} = [\boldsymbol{J}]^{-\mathrm{T}}\hat{\boldsymbol{\gamma}}, \hat{\boldsymbol{\gamma}} \in \boldsymbol{S}^h(\hat{A})\right\} \tag{18}$$

Here, $\boldsymbol{S}^h$ is the rectangular rotated Raviart–Thomas space,

$$\boldsymbol{S}^h(\hat{A}) = \{\hat{\boldsymbol{\gamma}} = (\gamma_\xi,\gamma_\eta), |\gamma_\xi = a_1 + a_2\eta, \gamma_\eta = b_1 + b_2\xi\}$$

The essential assumption is that the shear interpolation for γ_ξ is linear in η, and for γ_η, linear in ξ. In terms of the reduction operation, the assumed strain may be expressed as,

$$\boldsymbol{\gamma}^h = (\nabla w^h - \boldsymbol{R}_h\boldsymbol{\beta}^h) = [\boldsymbol{J}]^{-\mathrm{T}}(\widehat{\nabla}w^h - \boldsymbol{R}_{\hat{A}}[\boldsymbol{J}]^{\mathrm{T}}\boldsymbol{\beta}^h),$$
$$(x,y) \in A_e$$

where,

$$\widehat{\nabla}w^h = \sum_{i=1}^{4} \widehat{\nabla}N_i w_i, \quad \widehat{\nabla}N_i = (N_{i,\xi},N_{i,\eta})$$

$$\boldsymbol{R}_{\hat{A}}[\boldsymbol{J}]^{\mathrm{T}}\boldsymbol{\beta}^h = \sum_{i=1}^{4}[\boldsymbol{R}_{\hat{A}}^i][\boldsymbol{J}_i]^{\mathrm{T}}\boldsymbol{\beta}_i$$

In the above, $[\boldsymbol{J}_i]$ is the Jacobian evaluated at node i, and,

$$[\boldsymbol{R}_{\hat{A}}^i] = \begin{bmatrix} |N_{i,\xi}| & 0 \\ 0 & |N_{i,\eta}| \end{bmatrix}$$

where $|N_{i,\xi}|$, and $|N_{i,\eta}|$, are the absolute values of the shape function derivatives.

3.2. Variational equation

A stabilized finite element formulation may then be stated as: Find $\boldsymbol{u}^h = (\boldsymbol{\beta}^h, w^h) \in \boldsymbol{V}_h \times W_h$ such that,

$$\mathscr{B}_h(\boldsymbol{u}^h,\boldsymbol{v}^h;\omega)=\mathscr{F}_h(\boldsymbol{v}^h),\quad \forall \boldsymbol{v}^h=(\boldsymbol{\alpha}^h,v^h)\in \boldsymbol{V}_h\times W_h \tag{19}$$

The symmetric, bilinear form is defined as,

$$\begin{aligned}\mathscr{B}_h(\boldsymbol{u}^h,\boldsymbol{v}^h;\omega)&=GIa(\boldsymbol{\alpha}^h,\boldsymbol{\beta}^h)-\omega^2\{\rho t(v^h,w^h)+\rho I(\boldsymbol{\alpha}^h,\boldsymbol{\beta}^h)\}\\&+\sum_{A_e\in\mathscr{M}_h}\left\{\left(\frac{G\kappa t^3}{t^2+\kappa\alpha h_e^2}\right)(\nabla v^h-\boldsymbol{R}_h\boldsymbol{\alpha}^h,\nabla w^h-\boldsymbol{R}_h\boldsymbol{\beta}^h)_{A_e}\right.\\&+\tau_1^e(\nabla\mathscr{L}_1(\boldsymbol{v}^h)+\rho t\omega^2\nabla v^h,\nabla\mathscr{L}_1(\boldsymbol{u}^h)+\rho t\omega^2\nabla w^h)_{A_e}\\&\left.+\tau_2^e(\mathscr{L}_2(\boldsymbol{v}^h)+\rho I\omega^2\operatorname{div}\boldsymbol{\alpha}^h,\mathscr{L}_2(\boldsymbol{u}^h)+\rho I\omega^2\operatorname{div}\boldsymbol{\beta}^h)_{A_e}\right\}\end{aligned} \tag{20}$$

The linear form is defined as,

$$\mathscr{F}_h(\boldsymbol{v}^h;\omega)=(v^h,f)-\sum_{A_e\in\mathscr{M}_h}\tau_1^e(\nabla\mathscr{L}_1(\boldsymbol{v}^h)+\rho t\omega^2\nabla v^h,\nabla f)_{A_e} \tag{21}$$

$$R_1^h(\boldsymbol{u}^h;\omega)=\mathscr{L}_1(\boldsymbol{u}^h)+(\rho t\omega^2)w^h+f \tag{22}$$

$$R_2^h(\boldsymbol{u}^h;\omega)=\mathscr{L}_2(\boldsymbol{u}^h)+(\rho I\omega^2)\operatorname{div}\boldsymbol{\beta}^h \tag{23}$$

$$\begin{aligned}\mathscr{L}_1(\boldsymbol{u}^h)&=(G\kappa t)\operatorname{div}(\nabla w^h-\boldsymbol{R}_h\boldsymbol{\beta}^h)\\\mathscr{L}_2(\boldsymbol{u}^h)&=D_b\nabla^2\operatorname{div}\boldsymbol{\beta}^h+(G\kappa t)\operatorname{div}(\nabla w^h-\boldsymbol{R}_h\boldsymbol{\beta}^h)\end{aligned}$$

Here, h_e is a measure of the element size and $\alpha\geqslant 0$ is a positive constant. The functions $\tau_1^e(\omega)\leqslant 0$ and $\tau_2^e(\omega)\leqslant 0$ multiplying the generalized least-squares terms, are frequency dependent local element stabilization parameters determined from dispersion analysis and designed to explicitly match, on a uniform mesh of square elements, the analytical wave number–frequency relation (both real and imaginary wave numbers) for Mindlin plates. A similar generalized least-squares technique was used in [19,20] to improved the frequency response accuracy of quadrilateral plate elements based on assumed stress fields in a modified Hellinger–Reissner variational principle.

Special cases:

(1) Setting $\tau_1=\tau_2=0$, $\alpha\neq 0$, reverts to the stabilized form of the MITC element given in Lyly et al. [9,14,15], here extended to frequency response analysis.
(2) Setting $\alpha=0$, $\tau_1\neq 0$, $\tau_2\neq 0$ reverts to the generalized least-squares, stabilized MITC element given in Thompson and Thangavelu [10,11].
(3) Setting both $\tau_1=\tau_2=0$, and $\alpha=0$, reverts to the underlying MITC4 element of Bathe and Dvorkin [8].

For square elements with the MITC strain interpolation operating on the bilinear approximations W_h and $\boldsymbol{V}_h$ defined in (12) and (13), the residuals simplify, $\mathscr{L}_1(\boldsymbol{u}^h)=0$, $\mathscr{L}_2(\boldsymbol{u}^h)=0$, and the variational problem reduces to,

$$\begin{aligned}\mathscr{B}_h(\boldsymbol{u}^h,\boldsymbol{v}^h;\omega)&=GIa(\boldsymbol{\alpha}^h,\boldsymbol{\beta}^h)-\omega^2\{\rho t(v^h,w^h)+\rho I(\boldsymbol{\alpha}^h,\boldsymbol{\beta}^h)\}\\&+\sum_{A_e\in\mathscr{M}_h}\left\{\left(\frac{G\kappa t^3}{t^2+\kappa\alpha h_e^2}\right)(\nabla v^h-\boldsymbol{R}_h\boldsymbol{\alpha}^h,\nabla w^h-\boldsymbol{R}_h\boldsymbol{\beta}^h)_{A_e}\right.\\&\left.+r_1^e(\nabla v^h,\nabla w^h)_{A_e}+r_2^e(\operatorname{div}\boldsymbol{\alpha}^h,\operatorname{div}\boldsymbol{\beta}^h)_{A_e}\right\}\end{aligned} \tag{24}$$

$$\mathscr{F}_h(\boldsymbol{v}^h;\omega)=(v^h,f)-\sum_{A_e\in\mathscr{M}_h}(\tau_1\rho t\omega^2)(\nabla v^h,\nabla f)_{A_e} \tag{25}$$

where

$$r_1^e=(\rho t\omega^2)^2\tau_1^e,\quad r_2^e=(\rho I\omega^2)^2\tau_2^e$$

For the MITC4 interpolations on distorted quadrilateral element geometries, the differential operators $\mathscr{L}_1(\boldsymbol{u}^h)$, $\mathscr{L}_2(\boldsymbol{u}^h)$, are not precisely zero, and the simplifications given in (24) are not strictly valid. However, in implementing the least-squares terms on nonuniform meshes, the effect of the relatively small mixed derivatives and nonzero Laplacian on the residuals is neglected and we revert to (24). Extensive numerical studies conducted in [10] verify that this assumption on distorted element meshes does not alter the enhanced accuracy achieved with proper selection of the stabilization parameters r_1^e and r_2^e.

3.3. Element stabilization matrices

Substituting the bilinear interpolations for w^h and $\boldsymbol{\beta}^h$, together with the assumed strain $\boldsymbol{\gamma}^h$ defined by the MITC4 interpolation, into the variational equation (24), leads to the following element matrices,

$$[\boldsymbol{K}^e-\omega^2\boldsymbol{M}^e+r_1^e(\omega)\hat{\boldsymbol{M}}_1^e+r_2^e(\omega)\hat{\boldsymbol{M}}_2^e]\boldsymbol{d}^e=\boldsymbol{f}^e \tag{26}$$

Here, $\boldsymbol{d}^e$ is the 12×1 vector of element nodal dof derived from

$$\boldsymbol{d}^e=\{\boldsymbol{v}^h(\boldsymbol{x}_i)\}=\{(w_i,\boldsymbol{\beta}_i)\},\quad i=1,\ldots,4$$

and $\boldsymbol{K}^e$ and $\boldsymbol{M}^e$ are the element stiffness and mass matrices, respectively. For isotropic materials, the stiffness may be split in terms of a bending and transverse shear part,

$$\boldsymbol{K}^e(\alpha)=D_b\boldsymbol{K}_b^e+D_s^e(\alpha)\boldsymbol{K}_s^e$$

$$D_b=\frac{Et^3}{12(1-\nu^2)},\qquad D_s^e=\frac{G\kappa t^3}{t^2+\kappa\alpha h_e^2}$$

In the above, α is the shear stabilization number.

The frequency independent matrices multiplied by the least-squares stabilization parameters (r_1, r_2) may be expressed as,

$$\hat{\boldsymbol{M}}_1^e = \int_{A_e} \{\boldsymbol{N}_{1,x}^{\mathrm{T}} \boldsymbol{N}_{1,x} + \boldsymbol{N}_{1,y}^{\mathrm{T}} \boldsymbol{N}_{1,y}\}\, \mathrm{d}A \tag{27}$$

$$\hat{\boldsymbol{M}}_2^e = \int_{A_e} (\boldsymbol{N}_{21,x} + \boldsymbol{N}_{22,y})^{\mathrm{T}} (\boldsymbol{N}_{21,x} + \boldsymbol{N}_{22,y})\, \mathrm{d}A \tag{28}$$

where $\boldsymbol{N}_1$, $\boldsymbol{N}_{21}$ and $\boldsymbol{N}_{22}$ are row vectors of bilinear basis functions defined by the interpolations (16) written in vector form,

$$w^h = \boldsymbol{N}_1 \boldsymbol{d}^e, \quad \beta_x^h = \boldsymbol{N}_{21} \boldsymbol{d}^e, \quad \beta_y^h = \boldsymbol{N}_{22} \boldsymbol{d}^e \tag{29}$$

Optimal stabilization parameters $r_1(\omega)$, and $r_2(\omega)$ are determined by matching the finite element wave number–frequency relation to the exact wave number–frequency relation, for a given wave angle relative to a uniform mesh of square plate elements.

4. Wave number–frequency dispersion relation

The homogeneous plate equations of motion admit solutions of the form,

$$w = w_0\, \mathrm{e}^{(\mathrm{i}\boldsymbol{k}\cdot\boldsymbol{x})}, \quad \boldsymbol{\beta} = \theta_0 \boldsymbol{v}\, \mathrm{e}^{(\mathrm{i}\boldsymbol{k}\cdot\boldsymbol{x})} \tag{30}$$

In the above, $\mathrm{i} = \sqrt{-1}$, k is the wave number, $\boldsymbol{k} = k[\cos\theta, \sin\theta]$ defines a wave vector in the direction of wave propagation, $\boldsymbol{v} = [\cos\theta, \sin\theta]$. Conditions for the allowed waves are obtained by substituting the assumed exponentials (30) into the homogeneous equations of motion (7) and (8) with $f = 0$. The result is the dispersion equation relating frequency ω to wave number k. Rooting this expression results in wave number solutions which occur in pairs: $\pm k_1(\omega)$ and $\pm k_2(\omega)$, see [19] for further details:

$$k_{1,2}(\omega) = \pm \frac{1}{\sqrt{2}} \sqrt{k_s^2 + k_p^2 \pm \sqrt{(k_s^2 - k_p^2)^2 + 4k_b^4}} \tag{31}$$

In the above,

$$k_p(\omega) = \omega/c_p, \quad k_s(\omega) = \omega/c_s, \quad k_b(\omega) = (\rho t \omega^2/D_b)^{1/4}$$

$$c_p = \left[\frac{E}{\rho(1-\nu^2)}\right]^{1/2}, \quad c_s = \left(\frac{G\kappa}{\rho}\right)^{1/2}$$

At frequencies below a cutoff frequency, the wave number pair $\pm k_1(\omega)$ occurs as purely real, while the pair $\pm k_2(\omega) = \pm \mathrm{i}|k_2(\omega)|$ is purely imaginary. The real wave number pair corresponds to propagating waves while the imaginary pair corresponds to evanescent waves characterized by exponential decay.

5. Optimal least-squares stabilization parameters

The least-squares stabilization parameters r_1 and r_2 are determined such that the finite element wave number pairs match the analytical wave number pairs $\pm k_1$ and $\pm k_2$ for a given orientation $\theta = \varphi$. This strategy for designing mesh parameters to match real propagating, and imaginary wave numbers, is similar to that used in the displacement based GGLS Timoshenko beam element proposed given in [21], here extended to quadrilateral plates. The mesh parameters $r_l^e = r_l(\omega, \varphi, h_e)$, $l = 1, 2$ are obtained in terms of the stiffness and mass coefficients of the underlying plate element, the analytical wave numbers $k_1(\omega)$, and $k_2 = \mathrm{i}|k_2(\omega)|$, selected wave angle φ, and element size h_e. With the optimal selection of wave angle φ, dispersion error is minimized over the periodic interval $\theta \in (0, 45)$. This periodic interval defines the wave number accuracy of all possible wave angles. A similar technique was used in [12,17], to select optimal GLS parameters for the multi-dimensional scalar Helmholtz equation.

General expressions for the stabilization parameters for the MITC4 plate element are given below, see [10] for further details.

$$r_1^e = \left(-e_2 + \sqrt{e_2^2 - 4e_1e_3}\right) \Big/ (2e_1), \quad r_2^e = -\frac{c_{21}r_1^e + c_{11}}{c_{31} + c_{41}r_1^e} \tag{32}$$

where $e_l = e_l(c_{ij})$, $l = 1, 2, 3$, are defined by,

$$\begin{aligned} e_1 &= c_{24}c_{12} - c_{14}c_{22} \\ e_2 &= c_{23}c_{12} - c_{13}c_{22} + c_{11}c_{24} - c_{21}c_{14} \\ e_3 &= c_{11}c_{23} - c_{21}c_{13} \end{aligned}$$

with coefficients $c_{1i} = c_i(k_1, \varphi)$, and $c_{2i} = c_i(k_2, \varphi)$, $i = 1, 2, 3, 4$, defined by substituting the analytic wave numbers $k = k_1(\omega)$ and $k = \mathrm{i}|k_2(\omega)|$ into the functions,

$$\begin{aligned} c_1 &= G_{11}G_{22} - G_{12}G_{12} \\ c_2 &= G_{22}H_{11} \\ c_3 &= G_{11}\hat{H}_{22} \\ c_4 &= H_{11}\hat{H}_{22} \end{aligned}$$

$$\begin{aligned} G_{11} &= z_{11} + z_{14}(c_x + c_y) + z_{17}c_xc_y \\ G_{12} &= s_x(c_yz_{18} + z_{15})\cos\varphi + s_y(c_xz_{18} + z_{15})\sin\varphi \\ G_{22} &= z_{22} + (c_xz_{25} + c_yz_{36})\cos^2\varphi \\ &\quad + (c_yz_{25} + c_xz_{36})\sin^2\varphi \\ &\quad + z_{28}c_xc_y - z_{38}s_xs_y\sin 2\varphi \\ H_{11} &= (4 - c_x - c_y - 2c_xc_y)/2 \\ \hat{H}_{22} &= a_1 + a_2/2 + 3a_3/4 \end{aligned} \tag{33}$$

$$
\begin{aligned}
a_1 &= 1 - c_x \cos^2\varphi - c_y \sin^2\varphi \\
a_2 &= c_y \cos^2\varphi + c_x \sin^2\varphi - c_x c_y \\
a_3 &= s_x s_y \sin 2\varphi
\end{aligned}
$$

$$
\begin{aligned}
c_x &= \cos(k_x h_e), \quad c_y = \cos(k_y h_e) \\
s_x &= \sin(k_x h_e), \quad s_y = \sin(k_h h_e)
\end{aligned} \tag{34}
$$

$$
k_x = k\cos\varphi, \quad k_y = k\sin\varphi
$$

For both real $k = k_1(\omega)$, and imaginary wave numbers $k = \mathrm{i}|k_2(\omega)|$, the parameters r_1 and r_2 are real-valued. For the imaginary wave number we use the relations, $\cos(\mathrm{i}|k_2|y) = \cosh(|k_2|y)$, and $\sin(\mathrm{i}|k_2|y) = \mathrm{i}\sinh(|k_2|y)$. In this case, G_{12} is imaginary, yet c_1 is real-valued. The local element size in (34) is taken as $h_e = \sqrt{A_e}$, where A_e is the area of a general shaped four-node quad element, or an average element size computed from a patch of similarly sized elements. While the definition for the mesh parameters r_1 and r_2 are derived from a dispersion relation on a uniform mesh, accurate solutions on nonuniform meshes are shown to be relatively insensitive to the precise definitions used (see [10]).

The coefficients $z_{ij}(\omega) = K_{ij} - \omega^2 M_{ij}$, in (33), are determined in closed-form, from the underlying plate stiffness and mass matrices $K_{ij} = [\boldsymbol{K}^e]_{ij}$, and $M_{ij} = [\boldsymbol{M}^e]_{ij}$, for a reference square element with side length h_e, see Appendix A. Note that for nonzero shear stability parameter $\alpha > 0$, then $K_{ij} = K_{ij}(\alpha)$, and $z_{ij} = z_{ij}(\omega, \alpha)$. In this case, the least-squares stabilization parameters $r_l^e = r_l(\omega, \alpha, \varphi, h_e)$, adjust accordingly to match the analytical wave numbers at a given angle φ. The optimal angle φ, used in the definition of r_1, r_2, is determined from selecting the value which minimizes dispersion error over the determining periodic interval $\theta \in (0, 45)$. We show in the next section, that for a positive shear stabilization parameter $\alpha > 0$, then $\varphi = 45/2 = 22.5°$ is optimal. Interestingly, this same value was determined to be the optimal angle for the two-dimensional scalar Helmholtz equation [12].

Consistent with the optimal mesh parameter definitions r_1 and r_2, derived from a dispersion relation on a uniform mesh, the stabilization matrices (27) and (28), may be computed in closed form, based on a square element side length h_e, i.e.,

$$
\hat{\boldsymbol{M}}^e(\omega) = r_1^e(\omega)\hat{\boldsymbol{M}}_1^e + r_2^e(\omega)\hat{\boldsymbol{M}}_2^e \tag{35}
$$

can be written in nodal block form as,

$$
\hat{\boldsymbol{M}}^e = \frac{1}{12}\begin{bmatrix} \boldsymbol{A} & \boldsymbol{B} \\ \boldsymbol{B} & \boldsymbol{A} \end{bmatrix}, \quad \boldsymbol{A} = \begin{bmatrix} \boldsymbol{a}_{11} & \boldsymbol{a}_{12} \\ \boldsymbol{a}_{12}^{\mathrm{T}} & \boldsymbol{a}_{11} \end{bmatrix},
$$
$$
\boldsymbol{B} = \begin{bmatrix} \boldsymbol{b}_{11} & \boldsymbol{b}_{12} \\ \boldsymbol{b}_{12}^{\mathrm{T}} & \boldsymbol{b}_{22} \end{bmatrix} \tag{36}
$$

with diagonal nodal blocks,

$$
\boldsymbol{a}_{11} = \begin{bmatrix} 8r_1 & 0 & 0 \\ 0 & 4r_2 & 3r_2 \\ 0 & 3r_2 & 4r_2 \end{bmatrix}, \quad \boldsymbol{a}_{12} = \begin{bmatrix} -2r_1 & 0 & 0 \\ 0 & -4r_2 & -3r_2 \\ 0 & 3r_2 & 2r_2 \end{bmatrix}
$$
$$
\boldsymbol{b}_{11} = \begin{bmatrix} -4r_1 & 0 & 0 \\ 0 & -2r_2 & -3r_2 \\ 0 & -3r_2 & -2r_2 \end{bmatrix},
$$
$$
\boldsymbol{b}_{12} = \begin{bmatrix} -2r_1 & 0 & 0 \\ 0 & 2r_2 & 3r_2 \\ 0 & -3r_2 & -4r_2 \end{bmatrix},
$$
$$
\boldsymbol{b}_{22} = \begin{bmatrix} -4r_1 & 0 & 0 \\ 0 & 2r_2 & 3r_2 \\ 0 & 3r_2 & -2r_2 \end{bmatrix}
$$

In [10], a slightly simplified stabilization matrix $\hat{\boldsymbol{M}}_2^e$ obtained by neglecting cross-coupling terms in (28) was considered. Both dispersion analysis and numerical results showed that the simplified matrix maintains wave number accuracy. However, for consistency with the divergence of the bending residuals in the least squares operator, we now prefer to use the consistent matrix defined in (28), and computed in closed-form from (36).

6. Wave number accuracy

To quantify wave number accuracy, we perform a complex valued dispersion analysis [16] of the stabilized MITC4 plate element with different combinations of stabilization parameters α and r_1, r_2. Assuming wave solutions similar to (30) for a uniform mesh of quad elements, a characteristic equation relating frequency ω, and an approximate numeric wave number k^h, is determined. The dispersion relation for the stabilized plate elements considered here, may be expressed as [10]:

$$
\mathscr{D}(k, \omega) := (G_{11} + r_1 H_{11})(G_{22} + r_2 \hat{H}_{22}) - G_{12}^2 = 0 \tag{37}
$$

Given a frequency ω prior to cutoff, and rooting the dispersion relation (37), we find two pairs of numeric wave numbers, one real pair $\pm k_1^h(\omega)$, and one imaginary pair, $\pm k_2^h(\omega) = \pm\mathrm{i}|k_2^h(\omega)|$, similar to the analytic wave number–frequency relation (31). The numerical wave numbers $k_{1,2}^h$ display anisotropic behavior in that they depend on the wave angle direction relative to the finite element mesh, i.e., $k^h = k^h(\omega, \theta)$. In contrast, the analytical wave numbers $k_{1,2}$, are isotropic, independent of wave angle. The stabilization parameters $r_{1,2}(\omega, \alpha, \varphi, h_e)$ are designed to match the analytical wave number at a chosen angle $\theta = \varphi$. By precise selection of this angle, the stabilization provides improved wave number accuracy over other angles. The following results show that for $\alpha > 0$, then $\varphi = 22.5$, provides the best accuracy. In contrast, for $\alpha = 0$, it was shown in [10], that $\varphi = 30$, is the best choice. In the following we denote the various

stabilization methods with $\alpha > 0$ and $r_{1,2}(\varphi > 0)$, by the notation, STAB(α, φ). The underlying MITC4 element is denoted as STAB$(0,0)$, where $\alpha = 0$, and the 0 in the second slot indicates zero values for $r_1 = r_2 = 0$.

The relative error of the numerical wave number divided by the analytic wave number, k^h/k is shown in Figs. 1 and 2 for a frequency range up to $f = 2\pi\omega =$ 8000 Hz. This upper limit corresponds to roughly four

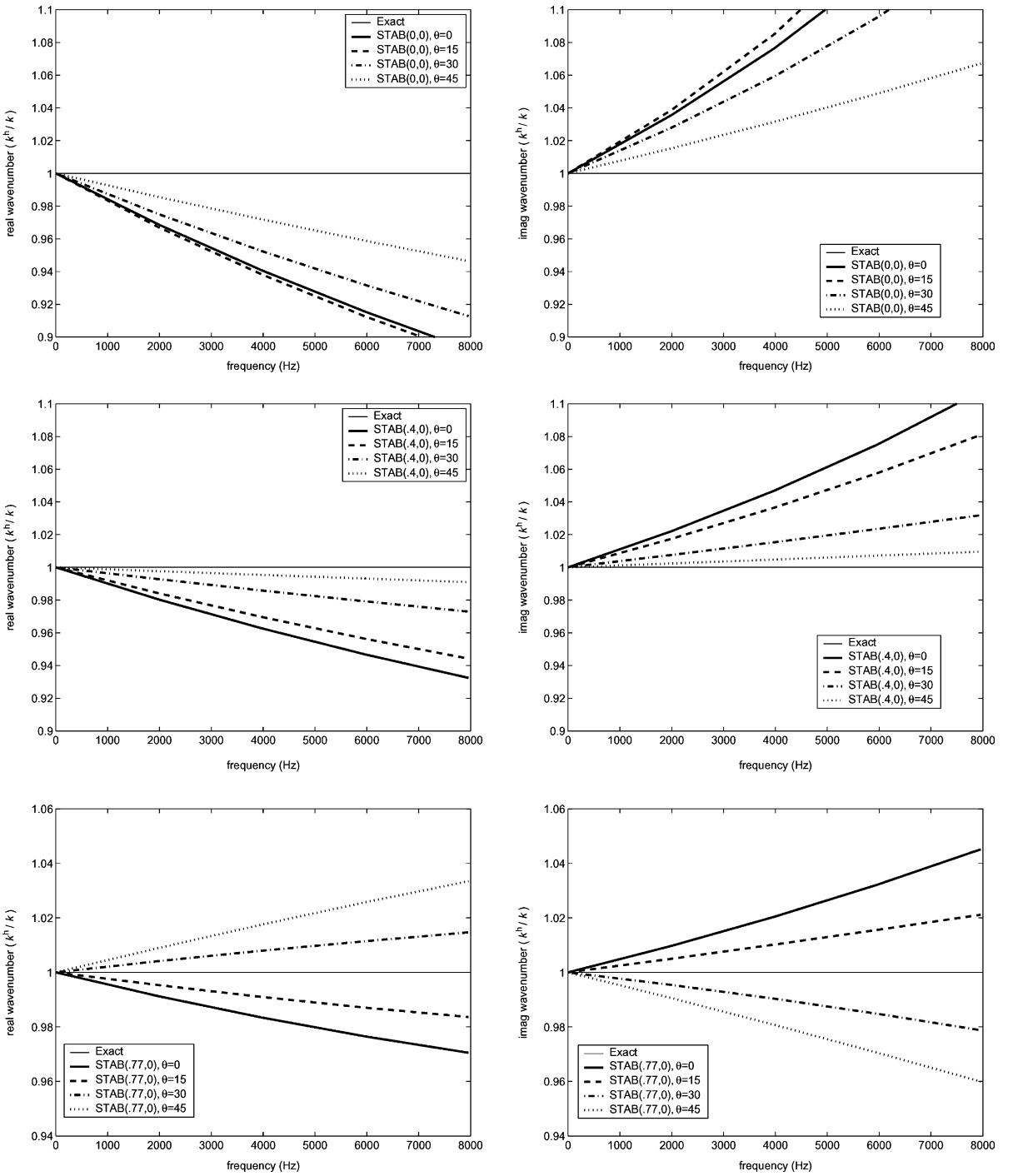

Fig. 1. Relative wave number error k^h/k at wave propagation angles $\theta = \{0°, 15°, 30°, 45°\}$. STAB($\alpha, 0$), $\alpha = \{0, 0.4, 0.77\}$, and $r_{1,2} = 0$. Left: real wave number k_1, right: imaginary wave number k_2.

elements per wavelength. Results correspond to a steel plate with properties: $E = 210 \times 10^{10}$ dynes/cm^2, $\nu = 0.29$, $\rho = 7.8$ g/cm^2, plate thickness $t = 0.15$ cm, and shear correction factor $\kappa = 5/6$. The square element side length is $h = 1.0$ cm. Results are plotted for equally spaced wave angles $\theta = 0°$, $15°$, $30°$ and $45°$. Due to symmetry, results are bounded by the extreme angles of $0°$ and $45°$, corresponding to waves directed along mesh

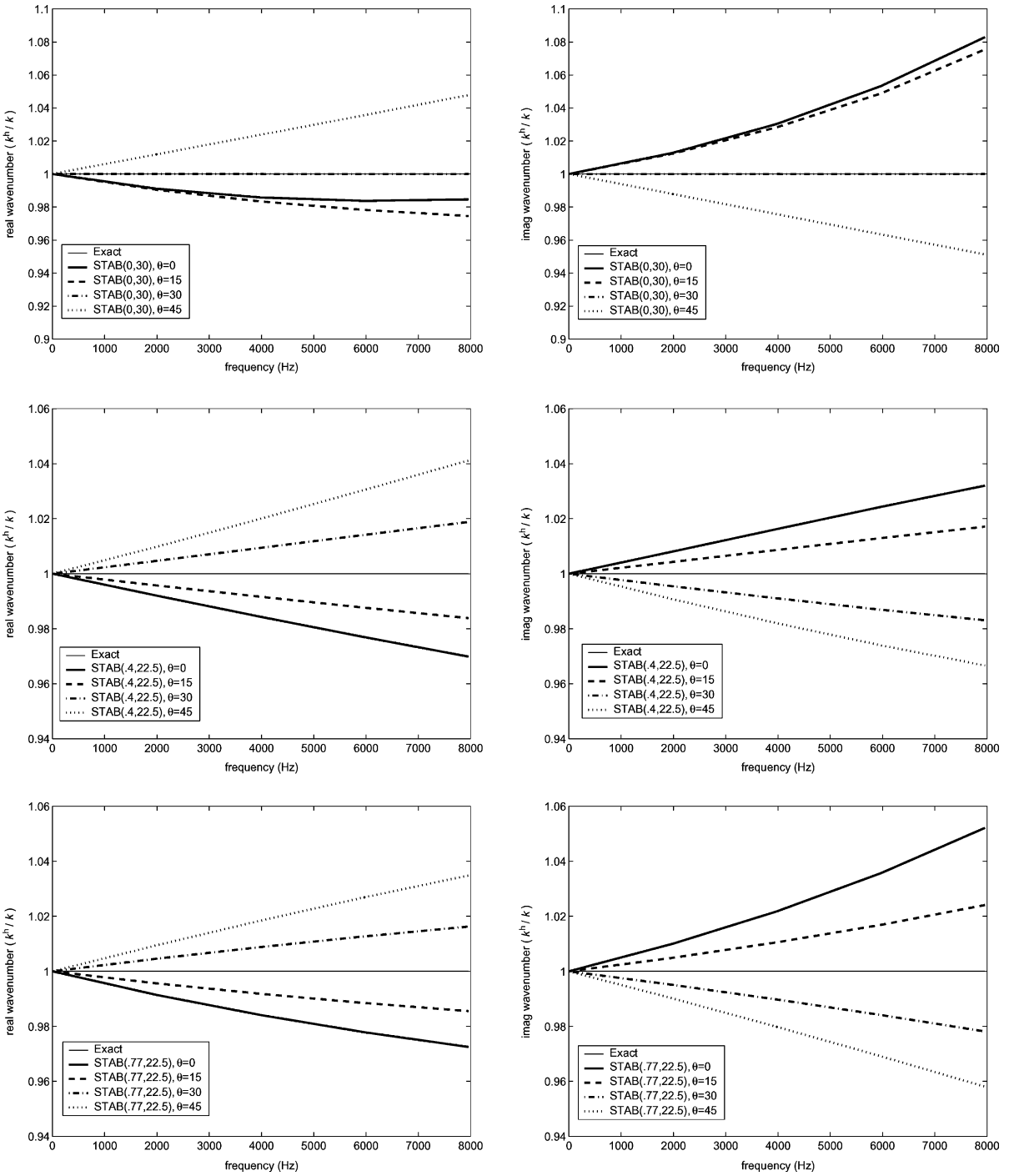

Fig. 2. Relative wave number error k^h/k at wave propagation angles $\theta = \{0°, 15°, 30°, 45°\}$. STAB$(\alpha, \varphi)$, $\alpha = \{0, 0.4, 0.77\}$, $r_{1,2}(\varphi = \{30, 22.5\})$. Left: real wave number k_1, right: imaginary wave number k_2.

lines and mesh diagonals, respectively. A ratio of $k^h/h = 1$, indicates exact wave number accuracy. Given the fixed mesh size, $h = 1$, as the frequency approaches the static case, $\omega \to 0$, wavelengths are increasing, relative to element size. In this region, the finite element solutions show improved wave number accuracy approaching $k^h/h \to 1$, resulting from the relative increase in the number of elements per wavelength.

For the MITC4 element, denoted STAB$(0,0)$ in the top of Fig. 1, the dispersion error is highest for waves approaching an angle of $\theta = 15°$, and then decreases after that, to a minimum error at $\theta = 45°$. At 1990 Hz, $k_1 = 0.73$, $\lambda = 2\pi/k_1 = 8.6$, which corresponds to 8.6 elements per wavelength, the maximum error is over 3%, both in the real propagating wave number k_1, and imaginary wave number k_2. At this level of mesh refinement relative to wavelength, the error in the propagating plate wave number k_1 is roughly double the dispersion error exhibited by the Galerkin finite element discretization for the scalar Helmholtz equation [12]. To achieve the accuracy level of the Helmholtz equation would require nearly twenty MITC4 plate elements per wavelength—a relatively high number. This observation illustrates the relatively poor accuracy of the MITC4 plate elements, motivating stabilized elements with improved wave number accuracy. As shown in the next section, reducing the percent error in the numerical wave numbers, even if by only a small amount, provides a significant overall increase in frequency response accuracy for forced vibration of plates.

The bottom two plots in Fig. 1 show the improved dispersion accuracy achieved for both the real and imaginary wave numbers by increasing only the shear stabilization parameter α, while keeping the generalized least-squares stabilization parameters $r_{1,2} = 0$. Starting with $\alpha \sim 0 > 0$, the maximum error decreases up to a value of $\alpha \sim 0.77$, but then increases for $\alpha > 0.77$. At the optimal value of $\alpha = 0.77$, the maximum error at 1990 Hz, is reduced to approximately 1%, a three-fold reduction in error compared to the underlying MITC4 element.

Further improvement is found by considering nonzero stabilization parameters $r_{1,2}$. Fig. 2 shows results for nonzero α, together with $r_{1,2}$ defined such that the numerical wave number matches the analytical wave number at the angle $\theta = \varphi = 45/2 = 22.5°$. With this selection, wave number error at the 0° and 45° angles is bisected, giving the best overall accuracy at all angles. Improved results occur over a wide range of α values with $r_{1,2}$ defined with $\varphi = 22.5$. At 1990 Hz, the maximum wave number error is approximately 1% over the wide range $\alpha \in (0.2, 0.77)$, in combination with nonzero $r_{1,2}$ defined with $\varphi = 22.5$. For the special case $\alpha = 0$, then $r_{1,2}$ defined with $\varphi = 30$, i.e., STAB$(0,30)$ = MLS4, gives best results, as reported as the mixed least squares (MLS4) element in [10]. We find that including shear stabilization $\alpha \in (0.2, 0.77)$, with $r_{1,2}$ defined with $\varphi = 22.5$, gives better results than the MLS4 element with $\alpha = 0$.

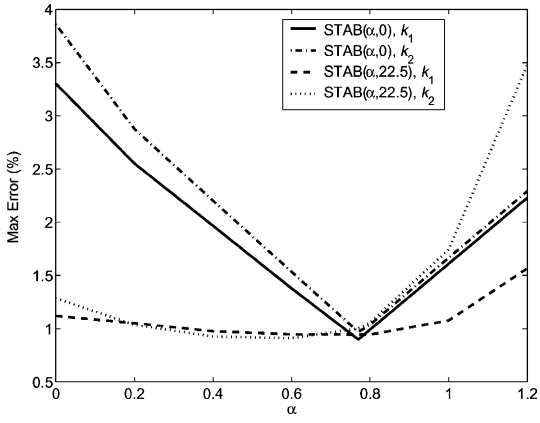

Fig. 3. Max error, $\max_{\theta\in(0°,45°)}(|k^h/k - 1| \times 100\%)$, as a function of shear stabilization number α, at 1990 Hz, corresponding to 8.6 elements per wavelength. Results shown, with $r_{1,2}$ stabilization defined with $\varphi = 22.5$, denoted STAB$(\alpha, 22.5)$, and without, denoted STAB$(\alpha, 0)$.

These observations are summarized in Fig. 3, which shows the maximum error defined over all wave angles given by,

$$\max \text{ error} = \max_{\theta\in(0°,45°)} \left(\left| \frac{k^h}{k} - 1 \right| \times 100\% \right)$$

Results are plotted as a function of α, with and without, $r_{1,2}$ stabilization, at 1990 Hz. At this discretization level relative to frequency (8.6 elements per wavelength), the least-squares stabilization defined by nonzero $r_{1,2}$ maintains an approximately 1% error over the entire range $\alpha \in (0, 0.77)$; beyond $\alpha > 0.77$, the error increases. Without $r_{1,2}$ stabilization, 1% error is only achieved at the select value $\alpha = 0.77$, and values just to the left or right show rapid increase in error.

7. Forced vibration example

To demonstrate the improved accuracy of the stabilized methods for frequency response analysis due to reduced wave number error, the problem of forced vibration of a simply supported steel plate with uniformly distributed time-harmonic pressure loading $f = 2$ dynes/cm^2, is examined. The plate is square with side length $L = 100$ cm. Material properties are the same as used for the dispersion analysis.

Using symmetry, only the upper-right 1/4 of the square is modeled with the unstructured mesh shown in Fig. 4 with an average element size of $h_{\text{ave}} = 1.115$. The local element size h_e, used to define the shear stabilization

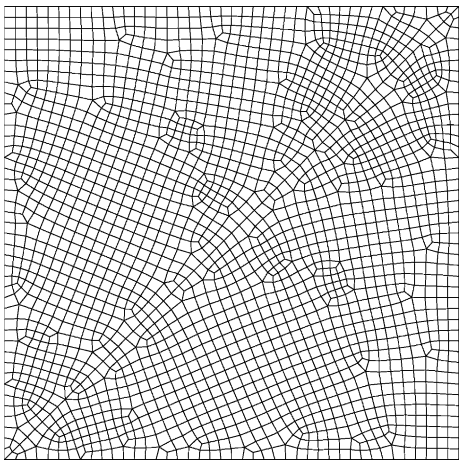

Fig. 4. Mesh generated with SDRC I-DEAS 'free-mesh' quad element algorithm: $n = 2095$ nodes, $N = 2010$ elements, $A = (50)^2$; average element size $h_{\text{ave}} = \sqrt{A/N} = 1.115$.

parameter $D_s^e(\alpha, h_e)$, and least-squares stabilization parameters $r_{1,2}^e(\omega, \alpha, \varphi, h_e)$, is computed for each element from the formula $h_e = \sqrt{A_e}$, where A_e is the quad element area.

To quantify error, we compute the discrete L_2 error measured over the entire plate, given by,

$$E^h(\omega) = \frac{\sqrt{\sum_{i=1}^{n} [w^h(x_i, y_i) - w(x_i, y_i)]^2}}{\sqrt{\sum_{i=1}^{n} [w(x_i, y_i)]^2}} \tag{38}$$

In the above, $w^h(x_i, y_i)$ is the finite element solution at a node point with coordinates (x_i, y_i), and $w(x_i, y_i)$ is the analytical series solution evaluated at the same point.

Fig. 5 shows the frequency response from 0 to 500 Hz, of the vertical deflection at the center of the plate, together with the global L_2 error. The results show that the underlying MITC4 element, denoted STAB$(0, 0)$ begins to show significant error beyond a driving frequency of 300 Hz. In contrast, the stabilized elements with combinations ($\alpha = 0.77$, $r_{1,2} = 0$), denoted STAB$(0.77, 0)$ and ($\alpha = 0.4$, $r_{1,2}(\varphi = 22.5)$), denoted STAB$(0.4, 22.5)$, show excellent accuracy over the entire frequency band. Results over the range $0.2 < \alpha < 0.77$, and least-squares stabilization $r_{1,2}(\varphi = 22.5)$, give simi-

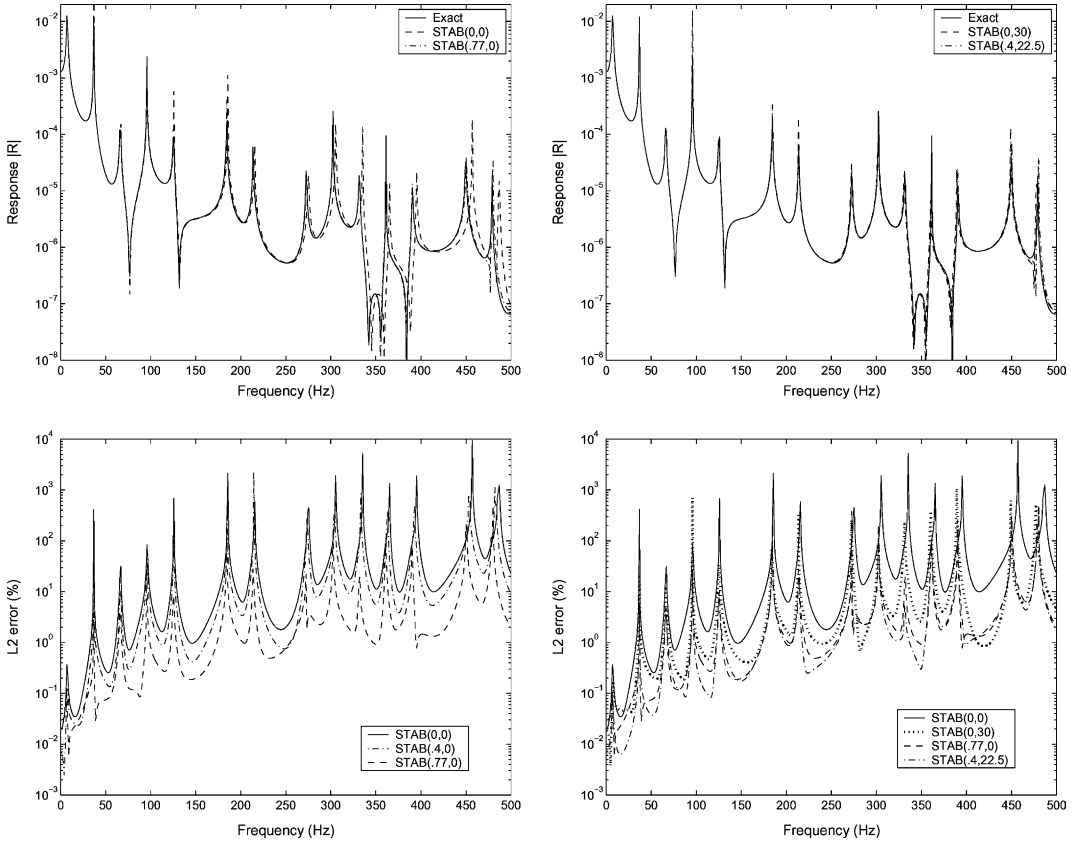

Fig. 5. Frequency window $f = 2\pi\omega \in (0, 500)$ Hz. Top: frequency response of vertical deflection at center of plate, $|R(\omega)| = |w_{\text{center}}(\omega)|$, bottom: relative L_2 error $|E^h(\omega)|$ over entire plate.

lar results to least-square stabilization case shown, defined with $\alpha = 0.4$. Solutions with $\alpha = 0, r_{1,2}(\varphi = 30)$, also give excellent accuracy; not shown.

Fig. 6 shows results over the higher frequency window, from 500 to 1000 Hz. Due to loss of wave number accuracy at these frequency levels, the MITC4 element shows significant error, completely misrepresenting resonance frequency locations. Results with stabilization, STAB$(0.77, 0)$, or STAB(α, 22.5), $\alpha \in (0.2, 0.77)$, show good accuracy. Fig. 7 shows that when optimal stabilization is used, accurate solutions are maintained all the way up to 2000 Hz. Fig. 8 shows the vertical deflection $\log_{10}(|w(s,\omega)|$, along the diagonal line of symmetry parameterized by coordinate $s = ((x-50)^2 + (y-50)^2)^{1/2}$, for the frequency range $f = 2\pi\omega \in (1000, 2000)$ Hz. Results for MITC4 show large errors in the frequency response solution. In contrast, the stabilized plate element solution closely matches the analytical series solution, over the entire frequency window. These results show the direct impact of improved wave number accuracy. A three-fold reduction in wave number error, translates to a three-fold increase in the frequency range over which accurate solutions are obtained.

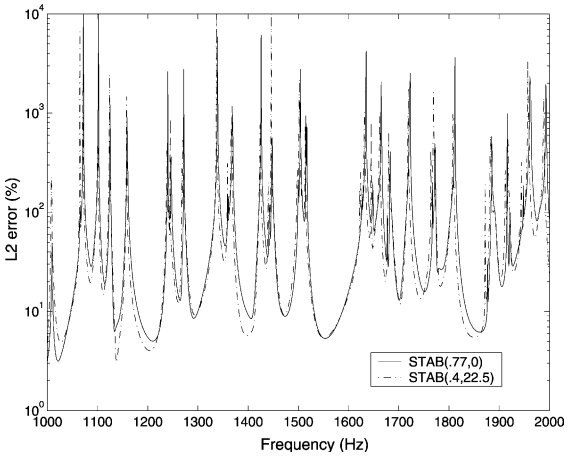

Fig. 7. Frequency window $f = 2\pi\omega \in (1000, 2000)$ Hz. Relative L_2 error $|E^h(\omega)|$ over entire plate.

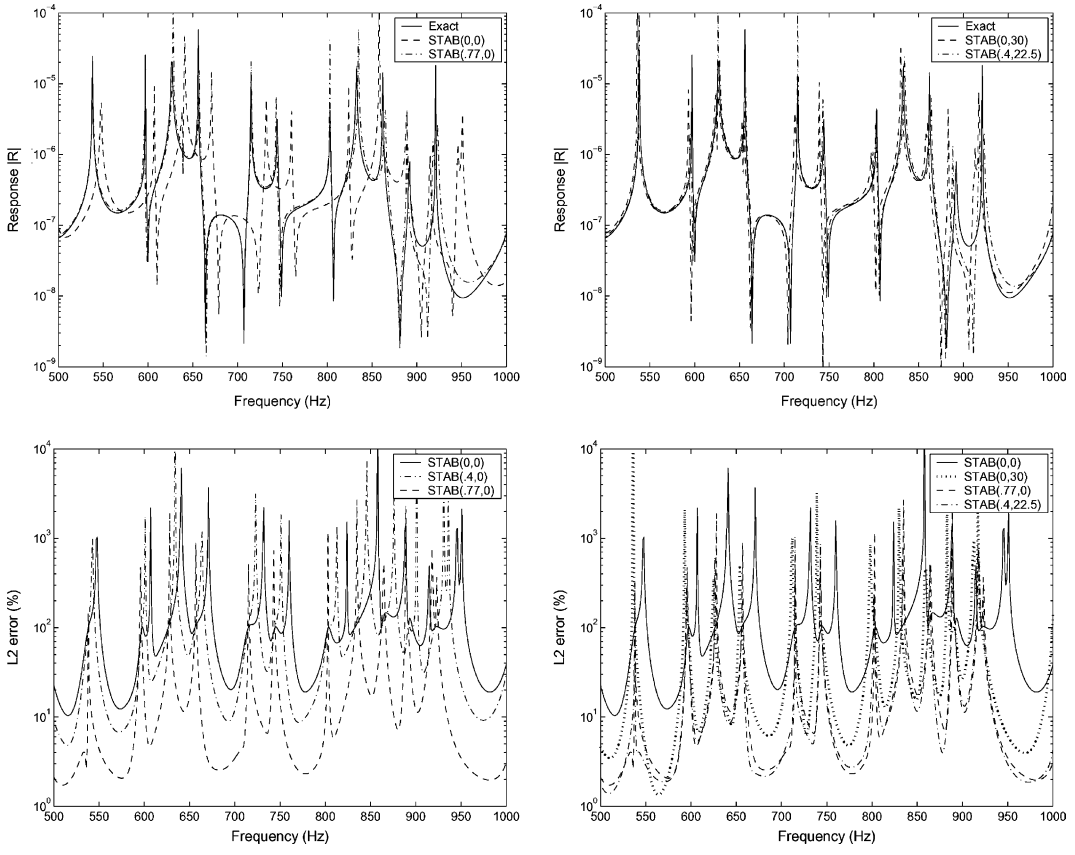

Fig. 6. Frequency window $f = 2\pi\omega \in (500, 1000)$ Hz. Top: frequency response of vertical deflection at center of plate, $|R(\omega)| = |w_{\text{center}}(\omega)|$, bottom: relative L_2 error $|E^h(\omega)|$ over entire plate.

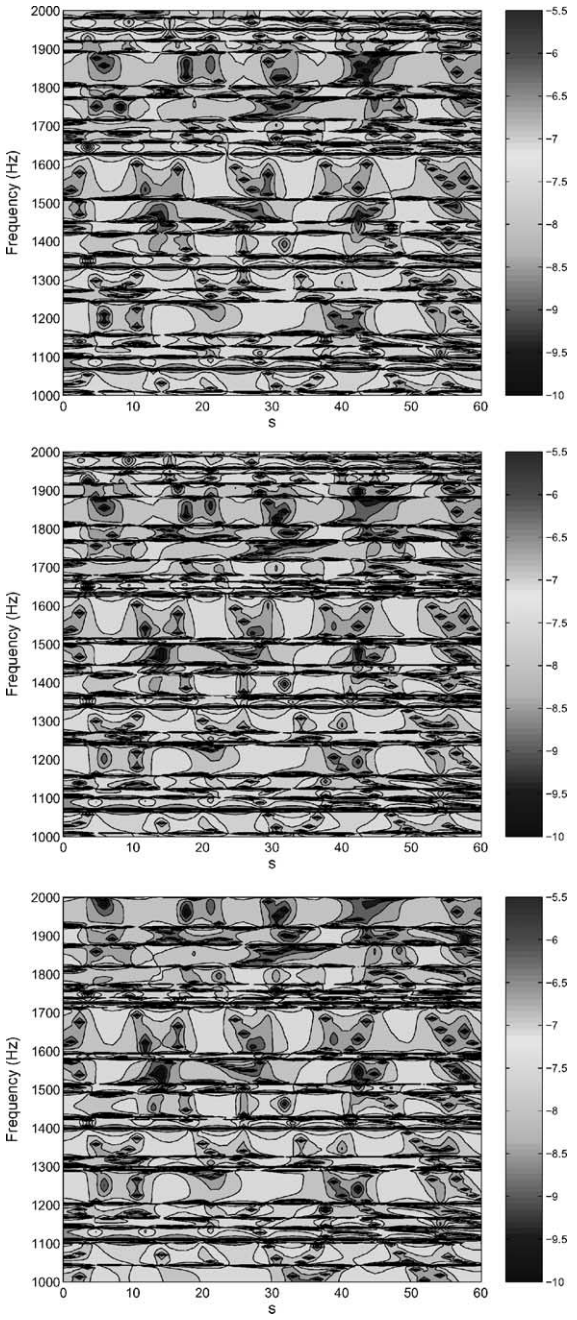

Fig. 8. Vertical deflection $\log_{10}(|w(s,\omega)|$, along the diagonal line of symmetry $s \in (0, 60)$, for the frequency range $f = 2\pi\omega \in (1000, 2000)$ Hz. Top: analytical series solution; middle: STAB$(0.4, 22.5)$; bottom: MITC4 = STAB$(0, 0)$.

8. Conclusions

Similar to the analytic dispersion relation for Mindlin plates, there are two pairs of numeric wave numbers $\pm k_1^h$, and $\pm \mathrm{i}|k_2^h|$, corresponding to propagating waves and exponential decay near drivers and discontinuities. MITC4 elements display relatively large errors in the wave number/frequency dispersion relation. For example, at frequencies corresponding to 8.6 elements per wavelength, the dispersion error in both the real propagating wave number, k_1, and imaginary wave number k_2, is greater than 3%. To achieve a 1.5% error would require over 20 elements/wavelength. Reducing the percent error in the numerical wave numbers, even if by only a small amount, provides a significant overall increase in frequency response accuracy.

By selecting the optimal number $\alpha = 0.77$, and element size defined as $h_e = \sqrt{A_e}$, where A_e is the element area, in the definition of the shear stabilization parameter $G_s^e(\alpha, h_e)$, wave number/frequency dispersion error is reduced by a factor of three. For example, at 8.6 elements per wavelength, the dispersion error in both k_1 and k_2 is only 1%. A more robust method is obtained by combining shear stabilization with the generalized least-squares stabilization defined by the local mesh parameters $r_{1,2}^e(\omega, \alpha, \varphi, h_e)$. Optimal stabilization parameters $r_{1,2}^e$ are determined such that the finite element wave number pairs $k_{1,2}^h$, match the analytical wave number pairs $k_{1,2}$ for a given wave orientation angle $\theta = \varphi$. For $\alpha > 0$, the optimal angle $\varphi = 22.5°$ is found to minimize dispersion error over all other angles. For example, with this value, at 8.6 elements/wavelength, the maximum wave number error over all wave angles and a wide range of shear parameter values $\alpha \in (0.2, 0.77)$, is maintained at approximately 1%. The significance of the least-squares stabilization, as defined by the optimal parameters $r_{1,2}^h(\omega, \alpha, 22.5, h_e)$, is that high accuracy is maintained and relatively insensitive to the precise definition of α and local element size h_e.

Numerical results for forced vibration frequency response, show that for a given mesh, the three-fold reduction in wave number error achieved by the stabilization methods directly translates to a three-fold increase in the frequency range over which accurate solutions are obtained, thus allowing for accurate solutions at significantly lower cost.

Future work includes extending the generalized least-squares methods developed here to shell elements with bending-membrane coupling.

Acknowledgements

Support for this work was provided by the National Science Foundation under Grant CMS-9702082 in conjunction with a Presidential Early Career Award for Scientists and Engineers (PECASE). We acknowledge the work of Klaus-Jürgen Bathe and colleagues in the derivation and mathematical analysis of the MITC strain interpolation for Mindlin plates, which serves as

the foundation for this work. I would also like to personally thank Klaus Bathe for his example and leadership in the development of finite element methods in computational mechanics. In particular I am thankful for his leadership in organizing the newly formed series MIT Conference on Computational Fluid and Solid Mechanics, and the Symposium on Teaching Mechanics and Finite Element Analysis, held at MIT, June 1997, where we first met.

Appendix A

Closed form dynamic stiffness matrix expressions, $z_{ij} = K_{ij} - \omega^2 M_{ij}$, for square MITC4 element used in definitions of stabilization parameters (r_1, r_2) in (33).

$$\boldsymbol{z} = D_b \boldsymbol{K}_b^e + D_s^e \boldsymbol{K}_s^e - \omega^2 \boldsymbol{M}^e$$

$$\boldsymbol{K}_b^e = \begin{bmatrix} \boldsymbol{A} & \boldsymbol{B} \\ \boldsymbol{B} & \boldsymbol{A} \end{bmatrix}, \quad \begin{aligned} t2 &= (3-v)/6 \\ t3 &= (1+v)/8 \\ t4 &= -(3+v)/12 \\ t5 &= (3v-1)/8 \\ t6 &= -t2/2 \\ t7 &= v/6 \end{aligned}$$

$$\boldsymbol{A}^{\mathrm{T}} = \begin{bmatrix} 0 & 0 & 0 & 0 & 0 & 0 \\ 0 & t2 & t3 & 0 & t4 & t5 \\ 0 & t3 & t2 & 0 & -t5 & t7 \\ 0 & 0 & 0 & 0 & 0 & 0 \\ 0 & t4 & -t5 & 0 & t2 & -t3 \\ 0 & t5 & t7 & 0 & -t3 & t2 \end{bmatrix},$$

$$\boldsymbol{B}^{\mathrm{T}} = \begin{bmatrix} 0 & 0 & 0 & 0 & 0 & 0 \\ 0 & t6 & -t3 & 0 & t7 & -t5 \\ 0 & -t3 & t6 & 0 & t5 & t4 \\ 0 & 0 & 0 & 0 & 0 & 0 \\ 0 & t7 & t5 & 0 & t6 & t3 \\ 0 & -t5 & t4 & 0 & t3 & t6 \end{bmatrix}$$

$$\boldsymbol{K}_s^e = \frac{1}{24} \begin{bmatrix} \boldsymbol{A} & \boldsymbol{B} \\ \boldsymbol{B} & \boldsymbol{C} \end{bmatrix}$$

$$\boldsymbol{A}^{\mathrm{T}} = \begin{bmatrix} 16 & 4h & 4h & -4 & 4h & 2h \\ 4h & 2h^2 & 0 & -4h & 2h^2 & 0 \\ 4h & 0 & 2h^2 & 2h & 0 & h^2 \\ -4 & -4h & 2h & 16 & -4h & 4h \\ 4h & 2h^2 & 0 & -4h & 2h^2 & 0 \\ 2h & 0 & h^2 & 4h & 0 & 2h^2 \end{bmatrix},$$

$$\boldsymbol{B}^{\mathrm{T}} = \begin{bmatrix} -8 & -2h & -2h & -4 & -2h & -4h \\ 2h & h^2 & 0 & -2h & h^2 & 0 \\ 2h & 0 & h^2 & 4h & 0 & 2h^2 \\ -4 & 2h & -4h & -8 & 2h & -2h \\ 2h & h^2 & 0 & -2h & h^2 & 0 \\ 4h & 0 & 2h^2 & 2h & 0 & h^2 \end{bmatrix}$$

$$\boldsymbol{C}^{\mathrm{T}} = \begin{bmatrix} 16 & -4h & -4h & -4 & -4h & -2h \\ -4h & 2h^2 & 0 & 4h & 2h^2 & 0 \\ -4h & 0 & 2h^2 & -2h & 0 & h^2 \\ -4 & 4h & -2h & 16 & 4h & -4h \\ -4h & 2h^2 & 0 & 4h & 2h^2 & 0 \\ -2h & 0 & h^2 & -4h & 0 & 2h^2 \end{bmatrix}$$

$$\boldsymbol{M}^e = \rho h^2 \frac{1}{36} \begin{bmatrix} \boldsymbol{A} & \boldsymbol{B} \\ \boldsymbol{B} & \boldsymbol{A} \end{bmatrix}, \quad \boldsymbol{A} = \begin{bmatrix} \boldsymbol{a} & \boldsymbol{b} \\ \boldsymbol{b} & \boldsymbol{a} \end{bmatrix}, \quad \boldsymbol{B} = \begin{bmatrix} \boldsymbol{c} & \boldsymbol{b} \\ \boldsymbol{b} & \boldsymbol{c} \end{bmatrix}$$

$$\boldsymbol{c} = \mathrm{diag}(t, t^3/12, t^3/12), \quad \boldsymbol{a} = 4\boldsymbol{c}, \quad \boldsymbol{b} = 2\boldsymbol{c}$$

References

[1] Mindlin RD. Influence of rotatory inertia and shear on flexural motions of isotropic, elastic plates. ASME J Appl Mech 1951;18:31–8.

[2] Bathe KJ, Brezzi F. On the convergence of a four-node plate bending element based on Mindlin/Reissner plate theory and mixed interpolation. In: Whiteman JR, editor. Proc Conf Math Finite Elements Appl V. New York: Academic press; 1985. p. 491–503.

[3] Bathe KJ, Brezzi F. A simplified analysis of two plate bending elements—the MITC4 and MITC9 elements. In: Pande GN, Middleton J, editors. Proc Int Conf Numer Meth Eng, (NUMETA 87). Dordrecht: Martinus Nijhoff; 1987.

[4] Bathe KJ, Bucalem ML, Brezzi F. Displacement and stress convergence of our MITC plate bending elements. Eng Comput 1990;7:291–302.

[5] Pitkaranta J. Analysis of some low-order finite element schemes for Mindlin–Reissner and Kirchhoff plates. Numer Math 1988;53:237–54.

[6] Brezzi F, Fortin M, Stenberg R. Error analysis of mixed-interpolated elements for Reissner–Mindlin plates. Math Models Meth Appl Sci 1991;1:125–51.

[7] Ibrahimbegovic A. Quadrilateral finite elements for analysis of thick and thin plates. Comput Meth Appl Mech Eng 1993;110:195–209.

[8] Bathe KJ, Dvorkin E. A four node plate bending element based on Mindlin–Reissner plate theory and mixed interpolation. Int J Numer Meth Eng 1985;21:367–83.

[9] Lyly M, Stenberg R, Vihinen T. A stable bilinear element for the Reissner–Mindlin plate model. Comp Meth Appl Mech Eng 1993;110:343–57.

[10] Thompson LL, Thangavelu SR. A stabilized MITC element for accurate wave response in Reissner–Mindlin plates. Comp Struct 2002;80:769–89.

[11] Thompson LL, Thangavelu SR. A stabilized MITC finite element for accurate wave response in Reissner–Mindlin plates. In: Bathe KJ, editor. Computational fluid and solid mechanics Proceedings First MIT Conference on Computational Fluid and Solid Mechanics, 12–15 June, 2001. Elsevier Science Ltd; 2001. p. 502–8.

[12] Thompson LL, Pinsky PM. A Galerkin least squares finite element method for the two-dimensional Helmholtz equation. Int J Numer Meth Eng 1995;38:371–97.

[13] MacNeal RH. A simple quadrilateral shell element. Comput Struct 1978;8:175–83.
[14] Stenberg R. A new finite element formulation for the plate bending problem, asymptotic methods for elastic structures. In: Ciarlet PG, Trabucho L, Viano JM, editors. Proceedings of the International Conference, Lisbon, Portugal, 4–8 October, 1993, ISBN 3-11-014731-9. Walter de Gruyter & Co; 1995.
[15] Lyly M, Stenberg R. The stabilized MITC plate bending elements. In: Proceedings of the Fourth World Conference on Computational Mechanics, Buenos Aires, 29 June–2 July, 1998.
[16] Thompson LL, Pinsky PM. Complex wave number Fourier analysis of the *p*-version finite element method. Computat Mech 1994;13(4):255–75.
[17] Harari I, Grosh K, Hughes TJR, Malhotra M, Pinsky PM, Stewart JR, et al. Recent developments in finite element methods for structural acoustics. Arch Computat Meth Eng 1996;3:132–311.
[18] Bathe KJ. Finite element procedures. Prentice-Hall; 1996.
[19] Thompson LL, Tong Y. Hybrid least squares finite element methods for Reissner–Mindlin plates. Comp Meth Appl Mech Eng, in press.
[20] Thompson LL, Sankar S. Dispersion analysis of stabilized finite element methods for acoustic fluid interaction with Reissner–Mindlin plates. Int J Numer Meth Eng 2001; 50(11):2521–45.
[21] Grosh K, Pinsky PM. Galerkin generalized least squares methods for Timoshenko beams. Comput Meth Appl Mech Eng 1996;132:1–16.